Ph.D. Dissertation of Medicine

# Evaluation of Radiation Sensitivity Differences in Mouse Liver Tumor Organoids using CRISPR/Cas9-mediated Gene Mutation

## 크리스퍼 유전자 가위를 이용한 마우스 간 종양 오가노이드의 방사선 반응성 탐색

August 2023

Graduate School of Medicine
Seoul National University
Radiation Oncology Major

Wan Jeon

# Evaluation of Radiation Sensitivity Differences in Mouse Liver Tumor Organoids using CRISPR/Cas9-mediated Gene Mutation

Dissertation Director In Ah Kim

Submitting a Ph.D. Dissertation of Medicine

April 2023

Graduate School of Medicine
Seoul National University
Radiation Oncology Major

Wan Jeon

Confirming the Ph.D. Dissertation written by Wan Jeon

July 2023

Chair _____(Seal)

Vice Chair _____(Seal)

Examiner _____(Seal)

Examiner _____(Seal)

Examiner _____(Seal)

# Abstract

# Evaluation of Radiation Sensitivity Differences in Mouse Liver Tumor Organoids using CRISPR/Cas9-mediated Gene Mutation

Wan Jeon

Graduate School of Medicine

Seoul National University

Radiation Oncology Major

As the development of cancer treatment, organoids have recently been used in various research fields. The creation of tumor organoid models through specific genetic mutations is opening up new horizons in patient care. In this study, to assess the radiation sensitivity of liver tumors harboring different genetic mutations, mouse liver tumors were generated in vivo through the hydrodynamic injection of clustered regularly interspaced short palindromic repeat/caspase 9 (CRISPR/Cas9) constructs encoding single-guide RNAs (sgRNAs) targeting *Tp53, Pten, Nf1, Nf2, Tsc2, Cdkn2a,* or *Rb1*.

The plasmid vectors were delivered via hydrodynamic tail vein injection to the liver of adult C57BL/6 male mice. The vectors were injected into 10 mice in each group. Organoids were generated from mouse liver tumors. The radiation response of the organoids was assessed using an ATP cell viability assay.

The mean survival period of mice injected with vectors targeting *Nf2* (4.8 months) was lower than that of other mice. Hematoxylin and eosin staining, immunohistochemical (IHC) staining, and target sequencing analyses revealed that mouse liver tumors harbored the expected mutations. Tumor organoids were established from mouse liver tumors. Histological evaluation revealed marked morphological similarities between the mouse liver tumors and the generated tumor organoids. Moreover, IHC staining indicated that the parental tumor protein expression pattern was maintained in the organoids. The results of the ATP cell viability assay revealed that the tumor organoids with mutated *Nf2* were more resistant to high-dose radiation than those with other gene mutations.

In this study, a radiation response evaluation system for mouse tumors with mutation target genes was developed using CRISPR/Cas9 and organoids. The *Tp53* and *Pten* double mutation in combination with the *Nf2* mutation increased the radiation resistance of tumors. The system used in this study can aid in elucidating the

mechanism underlying differential intrinsic radiation sensitivity of individual tumors. In the future, it can be considered as a method for predicting radiation therapy responsiveness according to genetic mutations of individual liver tumors in advance.

Keyword: CRISPR-Cas Systems, Liver, Organoids, Radiation Tolerance, Tumor

Student Number: 2017-38794

# Contents

# List of Table

# List of Figures

# Introduction

Liver cancer occurred in more than 900,000 people worldwide as of 2020, and is the 6th most common cancer in the world, the 5th most common cancer in men and the 9th most common cancer in women. Liver cancer also shows the second leading cause of cancer mortality (1).

Currently, various types of methods including surgery, trans-arterial chemoembolization (TACE), and radiation therapy are used as local treatments for liver cancer. The treatment of advanced liver cancer is also under development of various types of immune and targeted anticancer drugs. Nevertheless, studies on therapeutic models of liver tumors targeting specific gene mutations are currently limited.

The DNA revolution, clustered regularly interspaced short palindromic repeat-caspase 9 (CRISPR/Cas9) gene scissors, is a gene editing and gene screening tool that has recently been used in various studies. (2-5). CRISPR library screening has enabled the identification of various oncogenes and tumor suppressors in different types of cancer (5-7). However, the role of tumor

suppressor genes in accelerating the formation of liver cancer in different genetic backgrounds is not clear. Depending on the genetic background, mutations in tumor suppressor genes may differentially affect the progression of liver tumors.

Genomic landscape of liver cancer through biological engineering techniques such as next generation sequencing and CRISPR/Cas9 system technologies have revealed that specific genetic and molecular alterations are responsible for liver tumors. These findings are helping to point new therapeutic targets in immunotherapy and cancer treatment by targeting specific genetic mutations (8). Conversely, this can also be done with studies in which certain genetic mutations are caused by CRISPR/Cas9 gene editing and tumorigenicity is confirmed. It has been reported that co-mutation of *Tp53* and *Pten* genes using CRISPR/Cas9 can induce liver tumors in adult hepatitis B virus transgenic mice (9).

*TP53* is the most frequently mutated gene in human tumors. The liver-specific knockout of *Pten* promotes lipid accumulation and induces late-onset liver cancer in mice. Mutations in *TP53* and *PTEN* have been frequently reported in several types of human cancers, including human cholangiocarcinoma (10-12). In this study, mouse models were generated to determine the effect of mutations in tumor

suppressor genes on the acceleration of liver tumor formation in *Tp53*$^{-/-}$; *Pten*$^{-/-}$ genetic background.

Organoids are organ-specific cell aggregates made by aggregating and recombining cells isolated from stem cells or organ origin cells through a three-dimensional culture method. Organoid technology, a state-of-the-art cell culture tool, has revolutionized research on development, regeneration, and disease. The term 'organoid' was previously used to refer to various three-dimensional culture systems similar to organs modeled to varying degrees (13, 14). In 2013, Huch et al. developed a culture system of leucine-rich repeat-containing G protein-coupled receptor 5+ (Lgr5+) murine bile duct stem cell-derived organoids that can grow indefinitely in vitro (15). The authors generated clonal hepatocytes from human epithelial cell adhesion molecules+ (EpCAM+) cells around the adult bile duct (16). The aim of organoid research is to describe the developmental process and the organization of pathological organs in vitro to develop and test treatment options. The potential use of organoids in various clinical applications such as disease modeling, regenerative medicine, drug discovery, and personalized medicine has generated interest from the scientific community. Several studies have demonstrated

the application of organoids in anticancer drug sensitivity tests or radiation sensitivity tests (17, 18).

The method of genotyping clinical tumor samples and establishing radiotherapy strategies can be a new direction for personalized cancer treatment. Recently, personalized treatment according to individual characteristics of cancer has become a basic consideration in cancer treatment. The identification of the type and rate of mutated genes in the cancer tissues is a shortcut to personalized medicine.

This study used the CRISPR/Cas9 system to identify specific genetic mutations that cause an aggressive liver cancer phenotype and evaluated their effect on radiation sensitivity using organoids derived from mouse liver tumors generated.

# Material and Methods

## Experimental mice

Male C57BL/6 (aged 8-9 weeks) were purchased from Central Laboratory Animal Incorporated (Seoul, Korea). All animal protocols were approved by the Institutional Review Board (AEC-2017-009, AEC 2018-012). Reporting of this study conforms to ARRIVE 2.0 guidelines (19). The animal care protocols were based on the Guide for the Care and Use of Laboratory Animals, 8th edition (20).

## Construction of plasmids

To generate the CRISPR/Cas9 constructs, the px458 (Addgene #48138) plasmid that transiently expresses single-guide RNAs (sgRNAs) and wild-type SpCas9 was used. The sg*Tp53* sequence was inserted into the px458 plasmid and linearized using *Bbs*I. The U6 promoter and the sg*Pten* sequence were polymerase chain reaction (PCR)-amplified and inserted into the px458 plasmid encoding *Tp53* sgRNA. Next, the U6 promoter and sgRNAs targeting *Nf1*, *Nf2*, *Tsc2*, *Cdkn2a*, or *Rb1* were sequentially PCR-amplified and inserted into px458 encoding sgRNAs targeting *Tp53* and *Pten*. All primers used for cloning are listed in Table 1.

Table 1. Primers used in this study.[①]

| | | |
|---|---|---|
| gRNA | Pten-F | CACCGAGATCGTTAGCAGAAACAAA |
| | Pten-R | AAACTTTGTTTCTGCTAACGATCTC |
| | Tp53-F | CACCGCCTCGAGCTCCCTCTGAGCC |
| | Tp53-R | AAACGGCTCAGAGGGAGCTCGAGGC |
| | Nf1-F | CACCGTCCGAAGTTCGGCTGCATGT |
| | Nf1-R | AAACACATGCAGCCGAACTTCGGAC |
| | Nf2-F | CACCGCTTGGCGTCATATGCTGTCC |
| | Nf2-R | AAACGGACAGCATATGACGCCAAGC |
| | Tsc2-F | CACCGCACAGATCTGCCCTATCATT |
| | Tsc2-R | AAACAATGATAGGGCAGATCTGTGC |
| | Cdkn2a-F | CACCGGTGCGATATTTGCGTTCCGC |
| | Cdkn2a-R | AAACGCGGAACGCAAATATCGCACC |
| | Rb1-F | CACCGTTGGGAGAAAGTTTCATCCG |
| | Rb1-R | AAACCGGATGAAACTTTCTCCCAAC |
| *U6 promoter + sgRNA* | Nhe1-hU6 promoter F | AGTCGCTAGCGAGGGCCTATTTCCCATGAT |
| | Kpn1-XbaI-tracrRNA R | CAGTGGTACCTCTAGAGCCATTTGTCTGCAGAATTG |
| Deep sequencing primer | Pten-1st-F | ACACTCTTTCCCTACACGACGCTCTTCCGATCTCAGCTTCTGCCATCTCTCTCCT |
| | Pten-1st-R | GTGACTGGAGTTCAGACGTGTGCTCTTCCGATCTAGCAAAGAGGAACAGCCGC |
| | Tp53-1st-F | ACACTCTTTCCCTACACGACGCTCTTCCGATCTCTCTACAGATGACTGCCATGGAGGA |
| | Tp53-1st-R | GTGACTGGAGTTCAGACGTGTGCTCTTCCGATCTACAGGTATGGCGGGATGTATCTTAAG |
| | Nf2-1st-F | ACACTCTTTCCCTACACGACGCTCTTCCGATCTCTTTCAGGTGAAGAAGCAGATTTTGGAT |
| | Nf2-1st-R | GTGACTGGAGTTCAGACGTGTGCTCTTCCGATCTATAGCCATCCTGTGGAGTTAATGTTG |

① Table data was supported by Se Yeon Jung, Research Center, Dongnam Institute of Radiological and Medical Sciences, Busan, Republic of Korea.

## Generation of mouse liver tumor using CRISPR/Cas9

The CRISPR/Cas9 construct was delivered to the liver of adult C57BL/6 mice using hydrodynamic tail vein injection, which can deliver DNA to hepatocytes for transient expression (21). Plasmid constructs were extracted using the NucleoBond Xtra Maxi-EF kit (MN). The plasmids (60 μg) were prepared and diluted in 2 mL saline. The solution was hydrodynamically injected through the lateral tail vein using a 31-gauge syringe in 5-7 s (22). Plasmids with *Tp53+Pten*, *Tp53+Pten+Nf1*, *Tp53+Pten+Nf2*, *Tp53+Pten+Tsc2*, *Tp53+Pten+Cdkn2a*, or *Tp53+Pten+Rb1* sgRNAs were injected into 9-10 mice in each group. Mice were raised in a clean room to observe the development of liver tumors. The number of mice required in each experimental group was determined in a small-scale preliminary study and was based on the number of animals that died during the experiment and the minimum number of groups required to obtain the research data. Alfaxalone (60 mg/kg bodyweight) and xylazine (10 mg/kg bodyweight) were used as anesthetics for pain relief during euthanization. After the intraperitoneal injection, euthanasia was performed via asphyxiation using carbon dioxide gas (23).

## Survival analysis for The Cancer Genome Atlas (TCGA) data

Survival analysis and graph preparations were performed using the R (version 4.2.1) package "survival." (24, 25). Mice with *Tp53*+*Pten*, *Tp53*+*Pten*+*Nf1*, *Tp53*+*Pten*+*Nf2*, *Tp53*+*Pten*+*Tsc2*, *Tp53*+*Pten*+*Cdkn2a*, or *Tp53*+*Pten*+*Rb1* mutations were subjected to survival analysis. Clinical information on all tumor types was collected from TCGA. The retrieved information was filtered according to *TP53* and *PTEN* double mutation. The data on the expression levels of *NF1*, *NF2*, *TSC2*, *CDKN2A*, and *RB1* were collected from the cBioportal database. Survival analysis was performed according to each target gene by filtering only clinical information under low expression conditions.

## Histological evaluation and immunohistochemistry

To perform histological analysis, all the tumor tissues were fixed with 4% phosphate-buffered formalin, embedded into paraffin, and sectioned into 4-μm thick sections. The sections were stained with hematoxylin and eosin and imaged using a light microscope (Nikon Eclipse 80i; Nikon Corporation; Tokyo, Japan). The images were analyzed using J program software (NIH, Bethesda, MD, USA).

To perform immunohistochemical analyses, the tumor tissues were embedded in paraffin and sectioned into 4-μm thick sections. The tissue sections were blocked with goat serum for 1 h and incubated overnight with primary monoclonal antibodies against Tp53 (1:100, Santa Cruz Biotechnology, CA, #SC-126), Pten (1:200, Santa Cruz Biotechnology, #SC-7974), Nf2 (1:150; Santa Cruz Biotechnology, #SC-331), or Yap1 (1:50; Abcam, Cambridge, MA, #ab52771). Next, the sections were incubated with horseradish peroxidase-conjugated secondary antibodies using a diaminobenzidine substrate kit (Dako, Glostrup, Denmark). All sections were counterstained with Mayer's hematoxylin. The histological characteristics of the tumor

tissues were examined using an optical microscope (Nikon Eclipse 80i; Nikon Corporation, Tokyo, Japan).

## Organoid culture

For each liver sample, biopsies were obtained from non-tumorous or tumor tissues. The non-tumorous and tumor tissues were washed with Hank's balanced salt solution (HBSS; STEMCELL Technologies) and minced using sterile scalpel blades. The minced tissues were transferred into 50-mL conical tubes containing 30 mL of HBSS, inverted 10 times, and centrifuged at 350 *g* for 5 min (this step was repeated twice for washing). The tissues were resuspended in 8 mL of digestion buffer (7.2 mL HBSS, 800 μL collagenase P, and 80 μL DNAse I) at 230 rpm and 37° C for 40 min. The digestion was stopped with the addition of 10 mL HBSS. The samples were then centrifuged at 350 *g* for 5 min. The dissociated tissues were resuspended with 10 mL of HBSS and passed through a 70-μm cell strainer (Corning). Dissociated cell clusters (small pieces of tissues) were centrifuged. The pellet was resuspended in 100% Matrigel (Corning) and plated in a 120 μL drop in the middle of one well of a pre-coated 12-well plate (Corning). To allow solidification, the drop was incubated at 37° C and 5% $CO_2$ for 2 min. Next, 1 mL of the organoid culture isolation medium was added to the well for the initial 3-4 days, and the medium was replaced with the organoid culture

expansion medium. During culture, the medium was replaced once every three days. Organoids were passaged at a split ratio of 1:3 every 7-10 days. The organoid isolation medium comprises AdDMEM/F12 (Thermo Scientific, with 10 mM HEPES, 1× GlutaMax, and 1× penicillin-streptomycin) plus 2 nM Wnt surrogate-Fc Fusion protein (ImmunoPrecise), 25 ng/mL hNoggin (Peprotech), 5% RSPO1 conditioned medium (home-made), 1× B27, 50 ng/mL epidermal growth factor (Peprotech), 1 mM N-acetylcysteine (Sigma), 10 nM gastrin (Sigma), 50 ng/mL hepatocyte growth factor (Peprotech), 100 ng/mL FGF10 (Peprotech), 10 mM nicotinamide (Sigma), and 10 mM Rho inhibitor g-27632 (Calbiochem). After expansion, organoid isolation medium without 2 nM Wnt surrogate-Fc fusion protein (ImmunoPrecise) and 25 ng/mL hNoggin (Peprotech) was used. For tumoroid culture, the organoid expansion medium with 2 μM Nutlin-3 (Sigma) was used.

## Targeted deep sequencing

Targeted deep sequencing was performed as previously described (26). Briefly, genomic DNA from mouse liver organoids was isolated using the Wizard® genomic DNA purification kit (Promega). Genomic DNA was PCR-amplified using Phusion polymerase (New England Biolabs) with primers spanning the target sequence from approximately 75 bp upstream to 75 bp downstream of the cleavage site of CRISPR-Cas9. For the first round of PCR amplification, 100 ng of genomic DNA from each sample was used as a template. Meanwhile, for the second round of PCR amplification, 20 ng of purified PCR products from the first round of PCR amplification were annealed with both Illumina adapter and barcode sequences. The primers used for PCR are listed in Supplementary Table S1. The resulting products were isolated, purified, mixed, and subjected to 150 paired-end sequencing using the HiSeq system (Illumina). Deep sequencing data were sorted and analyzed with a reference wild-type sequence (no indel) using Cas-Analyzer (http://www.rgenome.net/cas-analyzer) with the comparison range (R) parameter, minimum frequency (n), and wild-type (WT) marker range (r) set to 50, 1, and 5, respectively (27). To increase accuracy,

the extracted data were filtered based on the read number. The read numbers of WT sequences (same target sequence but in different contexts because of sequencing errors) were combined as a single WT sequence.

## Cell viability assay after irradiation

The dome organoid was embedded and dislodged by pipetting with 1 mL organoid harvest solution (R&D Systems). The contents of the wells were transferred to a 15-mL tube and incubated on ice for 30 min. The samples were incubated with the same volume of phosphate-buffered saline and centrifuged at 1200 rpm for 5 min. The supernatant was aspirated and resuspended in pre-warmed TrypLE for 5 min with gentle pipetting to obtain a single-cell suspension. The single-cell suspension was transferred to microtubes (five groups for irradiation with 0, 1, 2, 4, and 8 Gy). Irradiation was performed using an electron beam from a 6 MeV C-band linear accelerator (28). The irradiated cells were centrifuged, and the supernatant was aspirated. The pellets were mixed with Matrigel and plated in a 120 μL drop in the middle of one well of a pre-coated 12-well plate (Corning) with organoid expansion media with or without Nutlin-3 for 7 days. Cell viability was assayed using CellTiter-Glo 3D (Promega), following the manufacturer's instructions, after 7 days of irradiation. Data analyses were performed using the GraphPad Prism 8 software.

## Statistical analyses

Data are presented as mean ± standard error. Cell viability assay data were analyzed using multiple t−tests to examine the effect of each radiation dose without assuming a consistent standard deviation. Statistical analyses were performed using GraphPad Prism 8 software. Differences were considered significant at $P < 0.05$.

# Results

## Generation of mouse liver tumor model

The generation of a mouse liver tumor model was observed. To investigate the effects of gene mutations, additional gene mutations were introduced in the *Tp53* and *Pten* double mutation background. *Tp53* and *Pten* double mutation is reported to induce liver tumors in approximately 4 months.[7] In this study, five known tumor suppressor genes (*Nf1*, *Nf2*, *Tsc2*, *Cdkn2a*, and *Rb1*) were selected (5, 6, 29). *Nf1*, *Nf2*, and *Tsc2* were selected as they have been identified as liver tumor suppressor genes through genome-wide ex vivo CRISPR screening in the *Tp53*$^{-/-}$ and Myc overexpression genetic background (6). *Cdkn2a* and *Rb1*, which are frequently mutated in human cancer, were selected as *CDKN2A* and *RB1* mutations co-occur with *TP53* mutation in human hepatocellular carcinoma (HCC) and/or bile duct cancer (29). To simultaneously introduce mutations in three genes, one vector system expressing three sgRNAs (sgTp53, sgPten, and sgRNA against target gene) was generated (Figure 1A). The CRISPR-Cas9 construct was delivered into mice via

hydrodynamic injection. After the generation of the liver tumor mouse model, liver tumor organoids were cultured and used for irradiation experiments to evaluate radiation sensitivity (Figure 1B).

Figure 1A. DNA constructs and overview of the experimental setup. Schematic map of the plasmid expressing three single-guide RNAs (sgRNAs) simultaneously. The sgRNA is expressed under the control of the U6 promoter, while the expression of spCas9 and enhanced green fluorescent protein is driven by the CBh (chicken beta-actin hybrid) promoter. A third sgRNA was introduced to target *Nf1, Nf2, Tsc2, Cdkn2a,* or *Rb1* along with the first and second sgRNAs to target *Tp53* and *Pten*, respectively. P2A, 2A self-cleaving peptide; pA; poly A signal.[②]

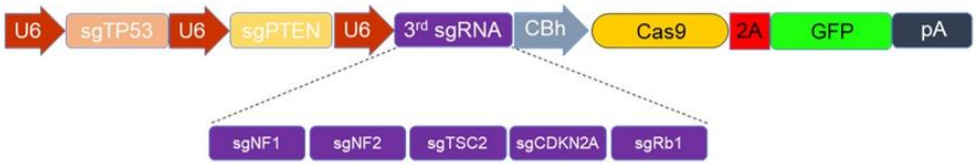


[②] Figure data was supported by Se Yeon Jung, Research Center, Dongnam Institute of Radiological and Medical Sciences, Busan, Republic of Korea.

Figure 1B. DNA constructs and overview of the experimental setup. Schematic representation of the experimental setup. After the establishment of the mouse tumor model through hydrodynamic tail vein injection of the clustered regularly interspaced short palindromic repeat-caspase 9 (CRISPR-Cas9) constructs, organoids were prepared from the generated mouse liver tumor to analyze their sensitivity to radiation.[③]

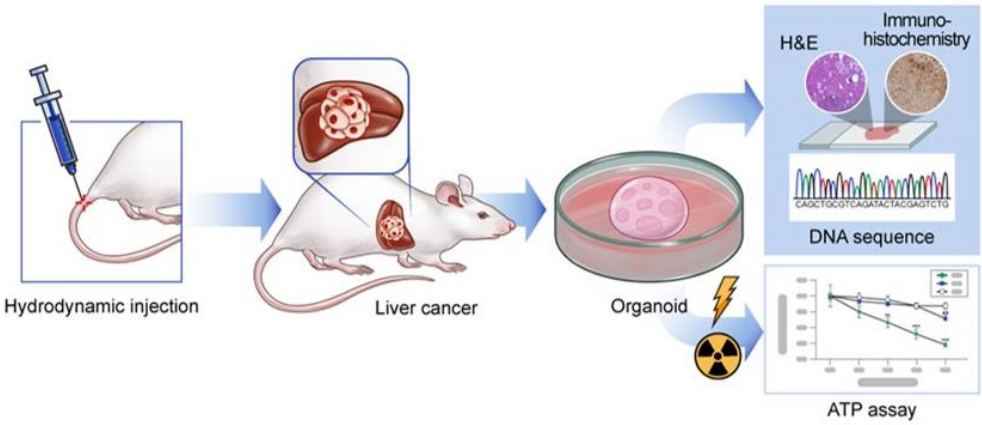


[③] This illustration was supported by Suhyun Chae in Ewha Medical Academy of Ewha Womans University Medical Center.

## Survival analysis for mouse model and human clinical data

The total survival period of mice according to the mutated gene was compared with human clinical data. The mouse survival period varied depending on the mutated genes in the *Tp53* and *Pten* double mutation background. Most mice with *Tp53* and *Pten* double mutation survived for 6 months post-hydrodynamic injection, whereas mice with *Tp53*, *Pten*, and *Nf2* triple mutation began to die 3 months post-hydrodynamic injection. Meanwhile, mice with *Tp53*, *Pten*, and *Tsc2* triple mutation began to die 4 months post-hydrodynamic injection (Figure 2A).

Figure 2A. Survival rates of mouse models and human cohort from The Cancer Genome Atlas (TCGA) datasets. Survival plots of mouse models with *Nf1, Nf2, Tsc2, Cdkn2a*, or *Rb1* mutations in the *Tp53* and *Pten* double mutation background. Significant differences in the survival rates between the six groups were examined using the log-rank test (P = 0.00042). Survival rate was significantly low in the *Tp53*+*Pten*+*Nf2* (n = 10) and *Tp53*+*Pten*+*Tsc2* (n = 10) groups. The *Tp53*+*Pten* (n = 9), *Tp53*+*Pten*+*Nf1* (n = 10), *Tp53*+*Pten*+*Cdkn2a* (n = 10), and *Tp53*+*Pten*+*Rb1* (n = 10) groups exhibited the same survival rate with overlapping survival curves.

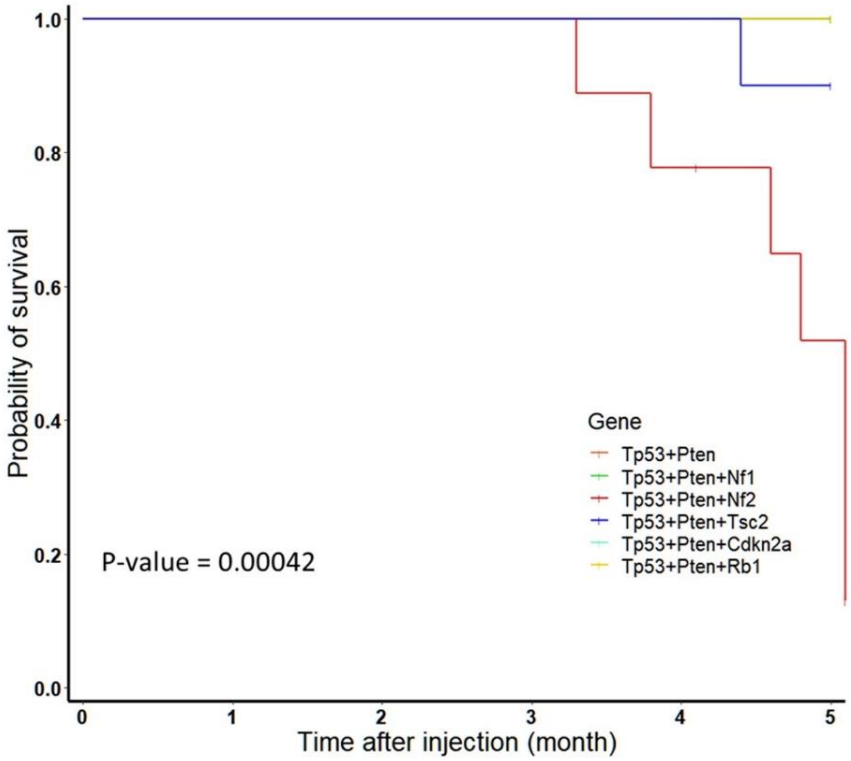

## Human data correlation

TCGA, a landmark cancer genomics program, was used to compare and analyze the relationship between mutated mouse genes and human clinical cancer data. To determine if the effects of mutations in five target genes (*Nf1*, *Nf2*, *Tsc2*, *Cdkn2a*, and *Rb1*) on tumor formation in mice are similar to those in humans, human clinical data were analyzed. In total, 10,967 human clinical datasets with *TP53* and *PTEN* mutations were retrieved from TCGA database. In the *TP53* and *PTEN* mutation genetic background, the number of samples with mutations in five genes (*NF1*, *NF2*, *TSC2*, *CDKN2A*, and *RB1*) was not sufficient for statistical analysis. Hence, the transcriptional data of the five genes were analyzed. The number of samples with downregulated expression of *NF1*, *NF2*, *TSC2*, *CDKN2A*, and *RB1* were 203, 174, 203, 123, and 206, respectively. As shown in Figure 2B, the survival rate in the groups with low *NF2* or *TSC2* expression was lower than that in other groups. These findings indicate a concordance in survival rates between mouse models and human clinical data.

Figure 2B. Survival rates of mouse models and human cohort from The Cancer Genome Atlas (TCGA) datasets. Survival plots for human clinical data with low expression levels of five genes (*NF1, NF2, TSC2, CDKN2A*, or *RB1*) in the cohort with *TP53* and *PTEN* double mutation background retrieved from TCGA database. Significance differences in the survival rates between the six groups were assessed using the log−rank test (P = 0.024, *PTEN*+*TP53* group not shown).④

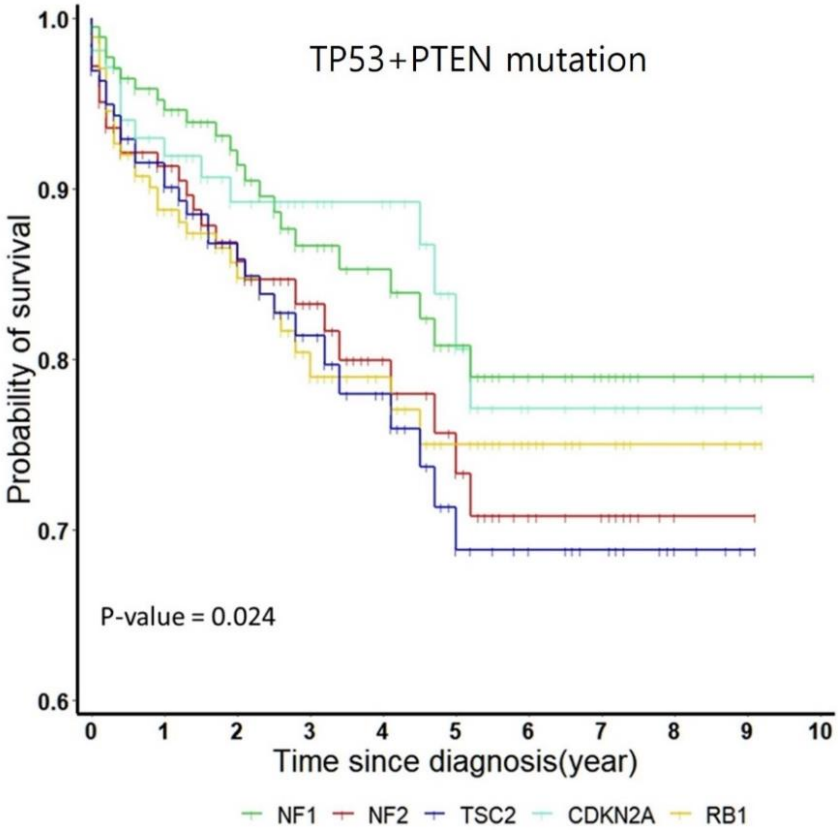


④ Figure data was supported by Chae Young Lee, Research Center, Dongnam Institute of Radiological and Medical Sciences, Busan, Republic of Korea.

## Tumor phenotype and immunohistochemical staining according to liver and lung metastases

The mouse liver and lung phenotypes according to the mutated genes were analyzed after the mice were sacrificed. As a result of observing gross changes in the liver according to each gene mutation, nodules were visible in the group with *Nf2* and *Tsc2* mutations in the background with *Tp53* and *Pten* double mutations. Mice, including those with lung metastases in the group in which liver tumors were established, were subjected to gross morphology and tissue analyses. Tumor formation was observed in all groups. This is consistent with the results of previous studies, which reported that *Tp53* and *Pten* double mutation induces liver tumors in approximately 4 months (21). *Nf2* or *Tsc2* mutation accelerated tumor formation in the *Tp53* and *Pten* double mutation background (Figure 2A). Therefore, liver tumor formation was further investigated in these two groups. The phenotypes of mouse liver, lung and retroperitoneal tumors (scale; 1 cm) according to each gene mutation (*Tp53*+*Pten*, *Tp53*+*Pten*+*Nf2*, and *Tp53*+*Pten*+*Tsc2*) are shown in Figure 3A–B. The differential histological characteristics between the tumor and the surrounding

non-tumor tissues were evaluated by subjecting the tissue sections (scale; 200 μm) to hematoxylin and eosin staining. The tumor tissue exhibited irregular infiltration in an undifferentiated state. *Nf2* can regulate the Hippo pathway and modulate the expression level of YAP1. Hence, this study examined *Nf2* mutation using immunohistochemical staining. Immunohistochemical staining revealed that the tumor exhibited an *Nf2*-negative phenotype when compared with the surrounding healthy liver stromal tissue (Figure 3C).

Figure 3A. Gross image of mouse liver and lung according to each gene mutation. Representative images of three groups with nodules and hematoxylin and eosin staining of tumors with *Tp53*+*Pten*, *Tp53*+*Pten*+*Nf2*, and *Tp53*+*Pten*+ *Tsc2* mutations.

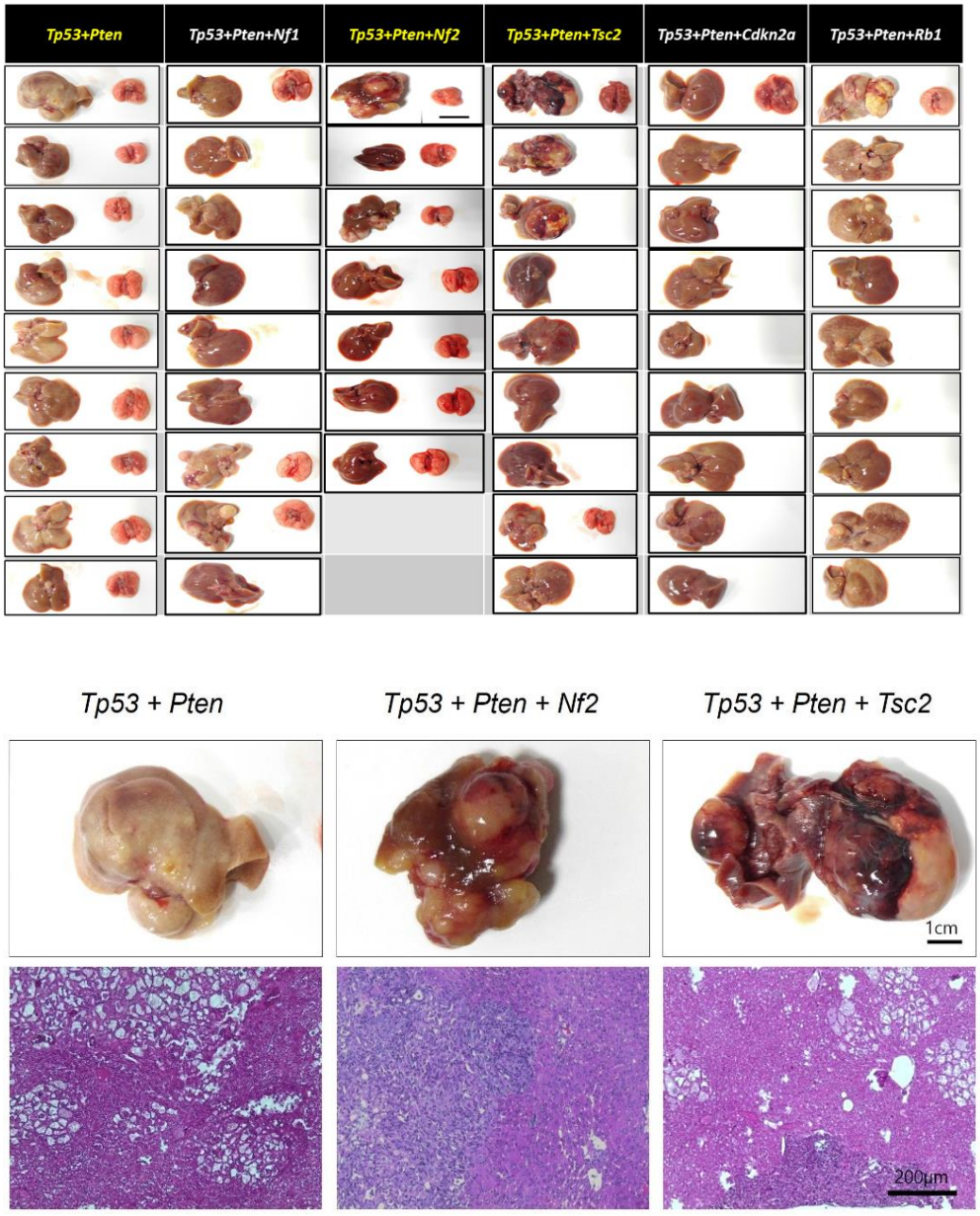

Figure 3B. Representative images of lung metastatic tumors with different gene mutations. Gross morphology, nodule phenotypes, and hematoxylin and eosin staining of lung metastatic tumors with *Tp53*+*Pten* and *Tp53*+*Pten*+*Tsc2* mutations.

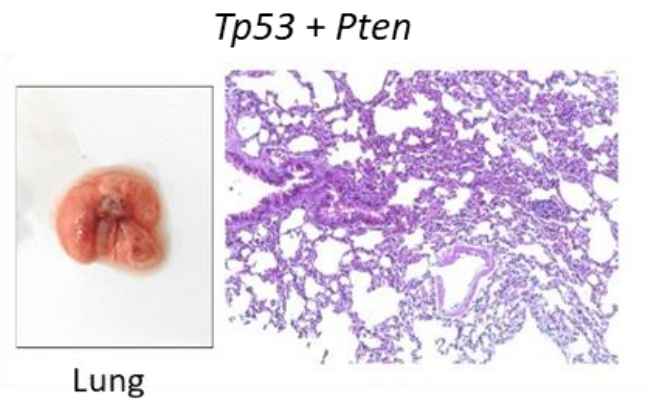


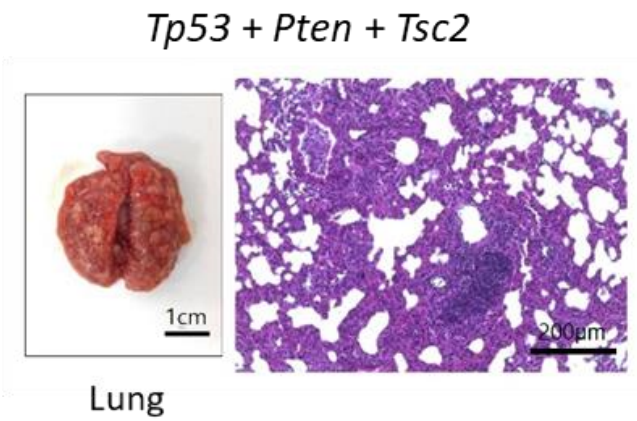

Figure 3C. Representative images of tumors with different gene mutations. Immunohistochemical analyses of Tp53, Pten, Nf2, and Yap1. Staining of other stromal cells in the liver served as a positive control.

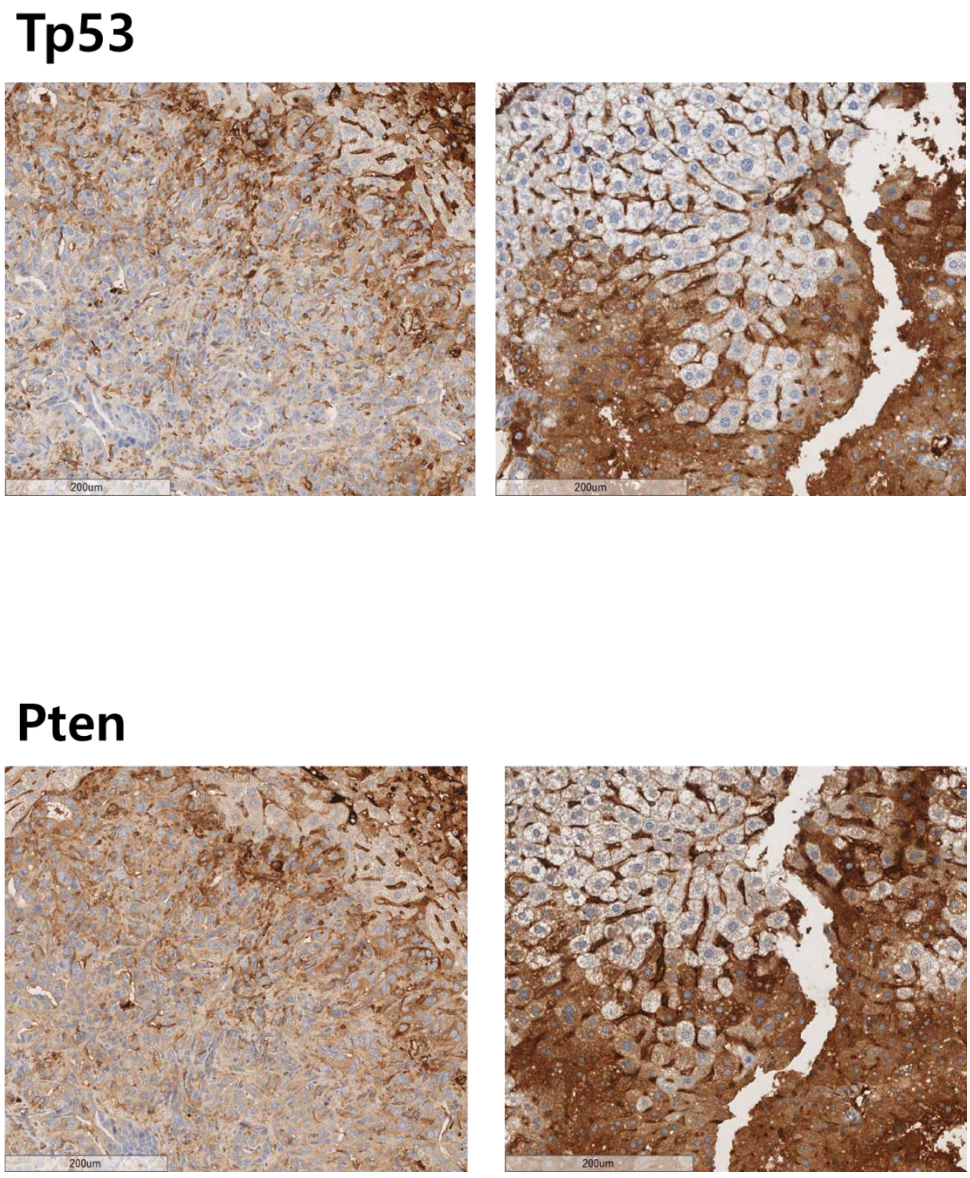

## Nf2

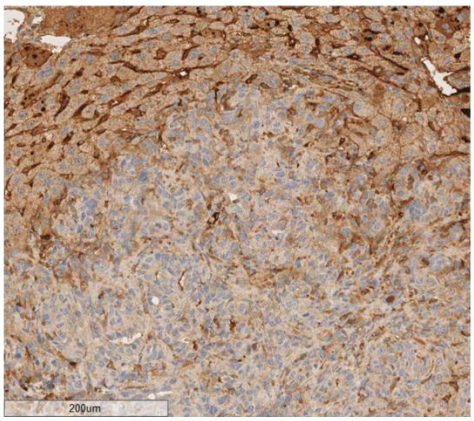


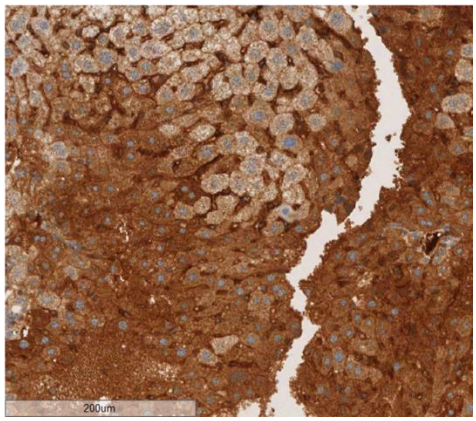


## Yap

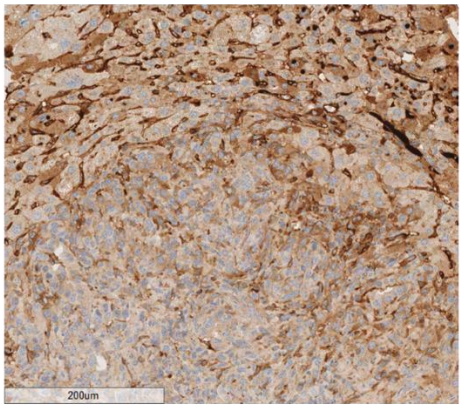


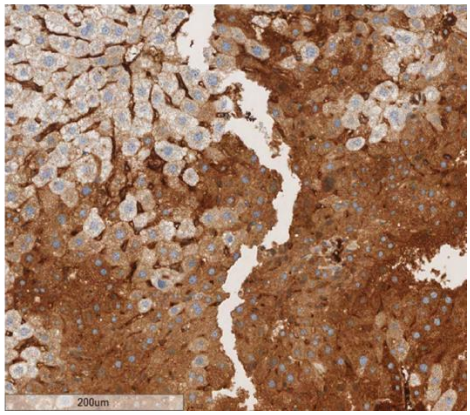

## Establishment of clonal *Tp53*+*Pten* and *Tp53*+*Pten*+*Nf2* knockout mouse liver organoid lines

In consultation with a pathologist (Ju Yeon Song, MD, Dongnam Institute of Radiological and Medical Sciences, Busan, Republic of Korea.) tumor and normal parts of mouse liver tissues were distinguished. Tissue samples were obtained from surgically resected and histologically diagnosed non-tumorous and tumorous liver tissues. The culture was initiated using the same organoid medium for 4 days. After several days, the cultures were exposed to Nutlin-3 to select organoids with the mutant *Tp53*+*Pten* and *Tp53*+*Pten*+*Nf2* phenotypes. Figure 4A shows the representative images of non-tumorous and *Tp53*+*Pten* and *Tp53*+*Pten*+*Nf2* mutant organoids. These organoid lines exhibited differential morphological phenotypes. Non-tumorous and *Pten*+*Tp53* mutant organoids exhibited a cystic structure, whereas *Tp53*+*Pten*+*Nf2* mutant organoids exhibited a compact morphology with no lumen. Targeted deep sequencing was performed to analyze the indel frequencies of candidate genes using CRISPR-Cas9 in single-cell-mediated mouse liver organoids. The CRISPR-Cas9 construct was

highly mutated near the cut site of the spacer (average 99.27% mutation, Figure 4B). Consistently, DNA sequencing confirmed that organoids with *Nf2* mutation were well established, whereas organoids with *Tsc2* mutation were not well established.

Figure 4A. Representative images of organoids. Mouse liver organoids with *Tp53*+*Pten* and *Tp53*+*Pten*+*Nf2* mutations after plating. Scale bar: 20 μm

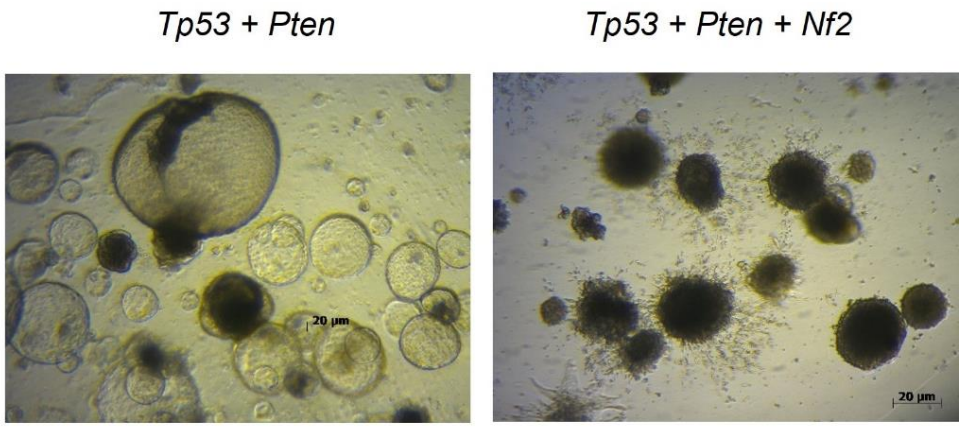

Figure 4B. Sequence analysis of representative indel patterns induced by clustered regularly interspaced short palindromic repeat-caspase 9 (CRISPR-Cas9) constructs. For each gene, the wild-type sequence is shown at the top containing the context sequence (indicated with gray text) and target sites (indicated with black text and highlighted in orange line). The PAM sequence is highlighted with a blue line. Deletions are shown as black dashes. The arrow indicates the cut site of the CRISPR-Cas9 construct. The mutation frequencies are shown on the right.[5]


[5] Figure data was supported by Se Yeon Jung, Research Center, Dongnam Institute of Radiological and Medical Sciences, Busan, Republic of Korea.

## Organoids with mutation exhibited differential sensitivity to radiation

To evaluate the response of the organoids to radiation, the organoids were irradiated with the indicated doses for 7 days. The cell survival rate was examined using CellTiter-Glo reagent. As shown in the bright-field images and cell survival rate results (Figure 5A-B), radiation dose-dependently exerted cytotoxic effects on non-tumorous organoids. In contrast, radiation did not exert cytotoxic effects on *Tp53+Pten* *Tp53+Pten+Nf2* mutant organoids at all tested doses, except at 8 Gy. These data indicated that patients with *Tp53*/*Pten*/*Nf2* mutation exhibit resistance to radiation therapy. In the non-irradiated group, organoid formation rate and size in the *Tp53+Pten+Nf2* group were lower than those in the *Tp53+Pten* group.

Figure 5A. Organoids exhibit differential sensitivity to radiation. Bright-field images of the organoids exposed to radiation at the indicated doses for 7 days are shown (control, *Tp53*+*Pten,* and *Tp53*+*Pten*+*Nf2*). Scale bar: 20 μm. This experiment was repeated two times in triplicate.

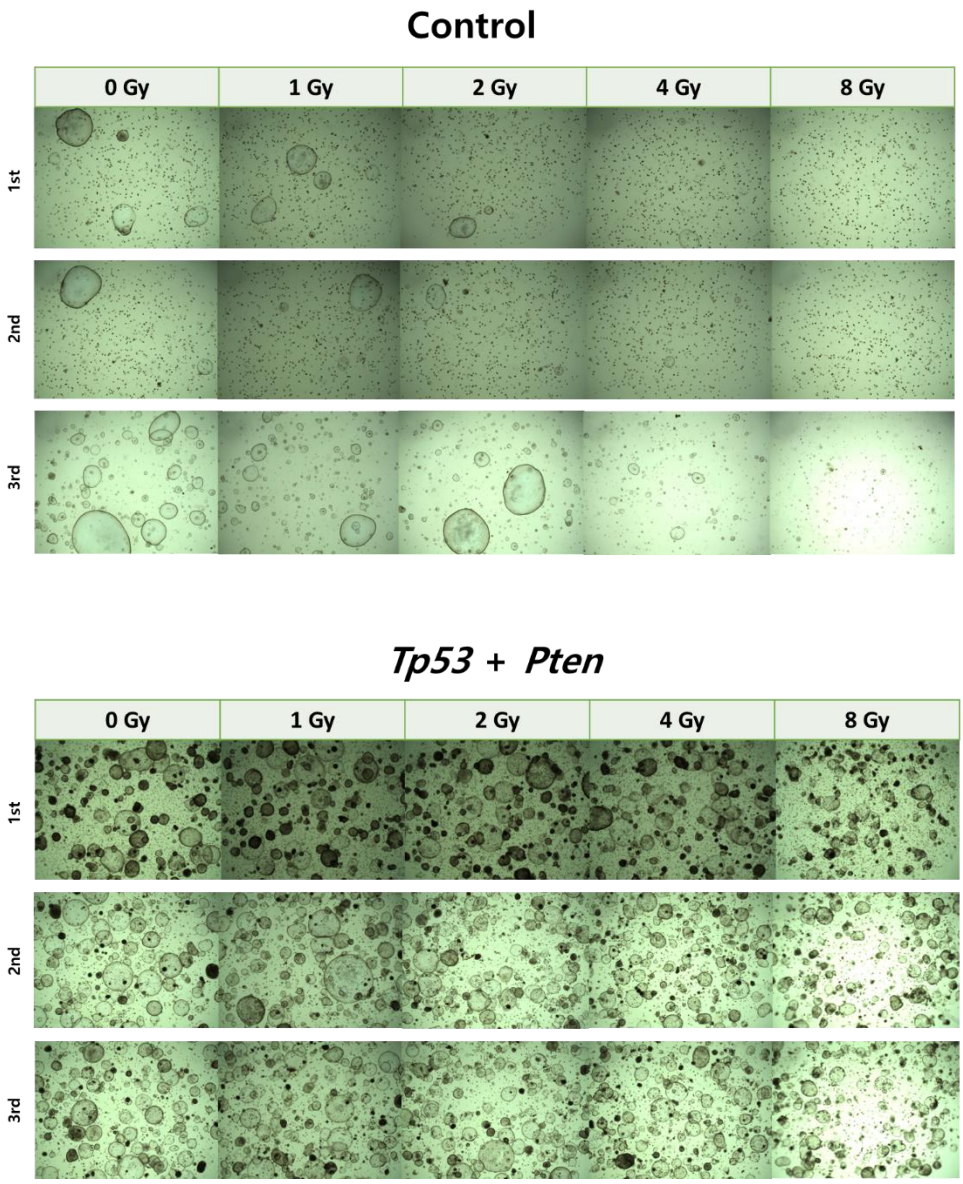

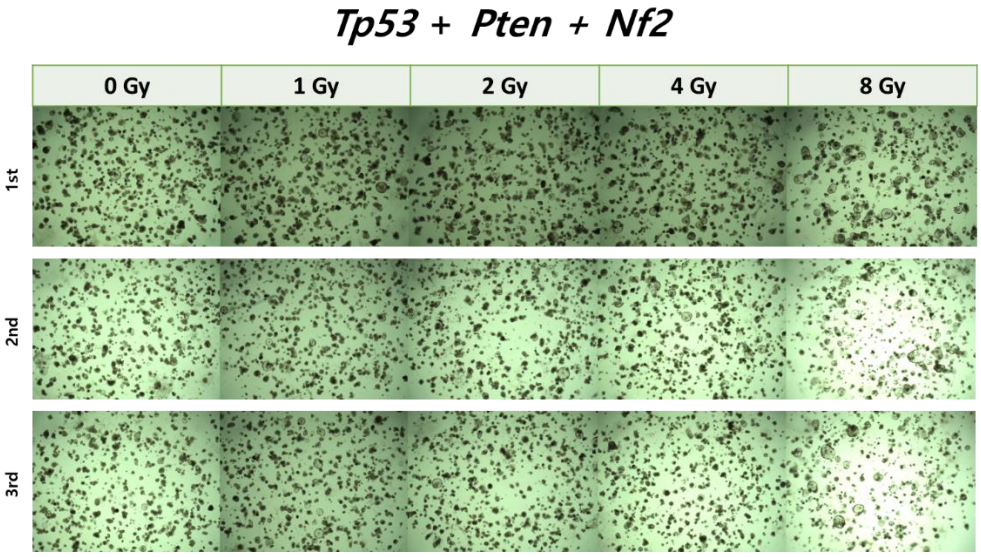
Tp53 + Pten + Nf2
0 Gy
1 Gy
2 Gy
4 Gy
8 Gy
1st
2nd
3rd

Figure 5B. Organoids exhibit differential sensitivity to radiation. Cell survival rate was recorded at day 7 post−irradiation. The results are expressed as mean ± standard error. **P < 0.01, ***P < 0.001 (control vs. *Tp53*+*Pten* or *Tp53*+*Pten*+*Nf2*) and ##P < 0.01 (*Tp53*+*Pten* vs. *Tp53*+*Pten*+*Nf2*). This experiment was repeated two times in triplicate.

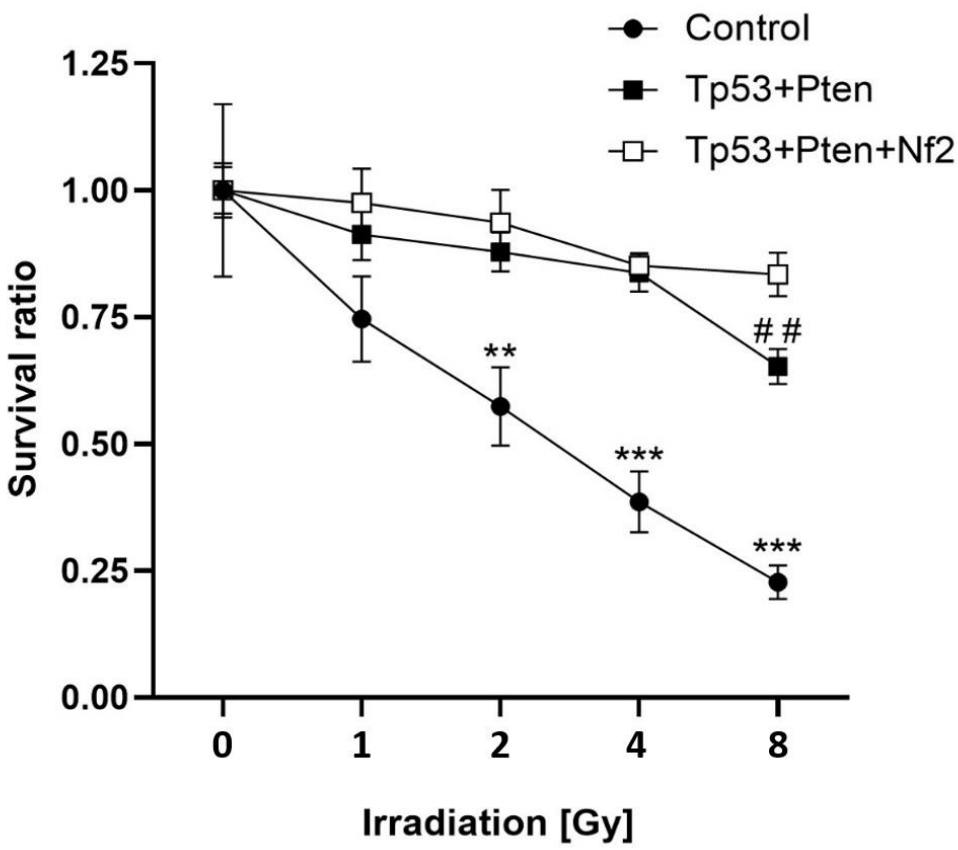

# Discussion

Currently, radiation therapy for liver tumors in clinical practice does not have different total dose and fraction schedules depending on genetic mutations of individual liver tumors. In that sense, tumor organoids are an important model for optimizing treatment strategies and examining the therapeutic mechanisms against cancer resistance. This is because mutated models can be generated using tumor organoids by focusing on a subset of the genetic characteristics of cancer (30). In this study, mouse liver cancer and its organoids were generated by introducing driver mutations in specific genes using the CRISPR/Cas9 gene editing system. Additionally, the effect of these mutations on radiation resistance was investigated (31). Cell viability assay revealed that the tumor organoid model with *Nf2* mutation in the *Tp53* and *Pten* double knockout background exhibited enhanced radiation resistance.

In hepatocellular carcinoma and intrahepatic cholangiocarcinoma, mutations in the *Nf2* gene are associated with the Hippo signaling pathway, play a key driver in cancer development through the Yap oncoprotein, and are known to be involved in tissue overgrowth (32,

33). Also, the *Nf2* gene has been reported to be involved in cytoskeleton development and microtubule stabilizing (34). In this study, organoids with additional mutations in the *Nf2* gene seemed to reflect the results of the above studies, and were morphologically more compact and showed fewer lumens than the groups with only *Tp53* and *Pten* gene mutations.

*PTEN* and *TP53* suppress stress factors associated with the tumorigenesis of liver cancer through distinct mechanisms. The simultaneous loss of both nuclear PTEN and TP53 promotes oxidative stress in hepatocytes, leading to the development of HCC and intrahepatic cholangiocarcinoma (35). Additionally, the deletion of *Nf2* in mouse HCC is known to modulate EGFR signaling and Hippo-dependent pathways and is functionally associated with the development of HCC (36).

As HCC exhibits an enormous variety of molecular properties, models with specific gene mutations can serve as research models that can consistently predict treatment responses. Particularly, the comparative analysis of radiation resistance of cancer organoid models with and without *Nf2* mutation can aid in predicting radiation resistance by introducing additional mutations in a specific gene, as well as in determining optimal treatment. Identifying genetic

mutations through tissue and genomic analysis of HCC can aid in establishing various personalized treatment strategies, including radiation therapy (37).

The effects of mutated tumor suppressor genes may vary depending on the genetic background. *Tp53*$^{-/-}$; Myc-overexpressing cells form tumors slowly but the inactivation of additional tumor suppressors accelerates tumor formation (6). In the *Tp53*$^{-/-}$; Myc overexpression genetic background, CRISPR-Cas9 screening revealed that *Nf1*, *Nf2*, *Tsc2*, and other genes accelerate tumor formation. Additionally, the findings of experiments with the *Tp53*$^{-/-}$; Myc overexpression; *Nf1*$^{-/-}$ mouse model, which was established via hydrodynamic injection, confirmed significant acceleration of liver tumor formation in mice (6). However, in this study, liver tumor formation was accelerated in mice with *Nf2* and *Tsc2* mutations but not in those with *Nf1* mutation in the *Tp53*$^{-/-}$; *Pten*$^{-/-}$ genetic background. This may be attributed to the epistatic network of interacting tumor suppressor genes. Zhao et al. reported that TP53 cooperated with NF2, and/or PTEN synergistically in breast cancer (7). Analysis of TCGA clinical dataset also reported that *NF2* mutation in the *TP53*$^{-/-}$; *PTEN*$^{-/-}$ genetic background accelerated tumor formation and affected overall survival. A combination of

mouse model and human clinical data analysis is useful for studying the effects of tumor suppressor genes on tumorigenesis in different genetic backgrounds.

A recent study used patient-derived tumor organoids to treat a rare type of primary liver cancer. The case was classified as HCC-neuroendocrine carcinoma and the best anticancer treatment option was suggested based on the establishment of organoids from the patient-derived tissues within 3 weeks after performing tissue and genetic analysis of HCC (38). Additionally, one study examined hepatitis B virus (HBV)-induced HCC using a liver organoid model. Customized and precise treatment was possible through analysis of genetic variations associated with the occurrence of liver cancer in HBV-infected patients (39).

The establishment of non-tumorous liver organoids and tumoroids from biopsies is advantageous because the models can be established at diagnosis, during treatment, and at the time of recurrence from minute amounts of biopsy material. The in vitro sensitivity of tumors to radiation was assayed in this study (Figures 4 and 5). These assays could provide a rationale for testing new therapies that are demonstrated to be effective in vitro and in vivo using the tumor tissue of the patient as an embedded source of information. Further

studies are needed to establish the usefulness of this approach, including a prospective evaluation of the concordance between patient and tumor responses to standard therapies, including chemotherapy and radiation therapy. In addition, after confirmation with a large sample size, an ex vivo radiation platform could be used to assess patient responses before initiating radiation treatment, which will potentially avoid the toxic side effects of radiation in patients with radiation-resistant tumors (40).

Accumulation of these data will contribute to devising various drug treatments, including immunotherapy targeting specific genes, through the elucidation of signaling pathways involved in the pathogenesis of HCC. The concept used in this study will aid in the elucidation of factors related to the differential intrinsic radiation sensitivity of individual tumors.

However, due to the nature of the organoid experiment in which blood vessels and immune cells do not exist, it will be limited to discuss the clinical significance of this experiment based only on the above results while excluding various factors that affect radiation sensitivity.

The limitations of this study are that the subject of the study is a mouse tumor model and small sample size. Hence, the applicability of the findings of mouse studies to human cancer models is limited. In addition, the tumor organoids generated in this study were confirmed using DNA sequencing. The *Nf2* mutant organoids exhibited good growth. However, the *Tsc2* mutant organoid model could not be established and hence its sensitivity to irradiation could not be determined.

# Conclusion

Through this study, it was confirmed that mouse liver tumors can be generated using CRISPR/Cas9 gene editing system. In addition, the radiation sensitivity of the generated liver tumors could be confirmed through an organoid model. The results of this study suggested the difference in response to irradiation according to genetic mutations in mouse liver tumor. For the clinical application of customized radiation therapy, liver tumor genome analysis of individual patients will be of great help in determining the direction of treatment.

# Reference


1. Sung H, Ferlay J, Siegel RL et al. Global Cancer Statistics 2020: GLOBOCAN Estimates of Incidence and Mortality Worldwide for 36 Cancers in 185 Countries. CA Cancer J Clin. 2021;71(3):209-49.
2. Mali P, Yang L, Esvelt KM et al. RNA-guided human genome engineering via Cas9. Science. 2013;339(6121):823-6.
3. Ran FA, Hsu PD, Wright J, Agarwala V, Scott DA, Zhang F. Genome engineering using the CRISPR-Cas9 system. Nat Protoc. 2013;8(11):2281-308.
4. Konermann S, Brigham MD, Trevino AE et al. Genome-scale transcriptional activation by an engineered CRISPR-Cas9 complex. Nature. 2015;517(7536):583-8.
5. Shalem O, Sanjana NE, Hartenian E et al. Genome-scale CRISPR-Cas9 knockout screening in human cells. Science. 2014;343(6166):84-7.
6. Song CQ, Li Y, Mou H et al. Genome-Wide CRISPR Screen Identifies Regulators of Mitogen-Activated Protein Kinase as Suppressors of Liver Tumors in Mice. Gastroenterology. 2017;152(5):1161-73 e1.

7. Zhao X, Li J, Liu Z, Powers S. Combinatorial CRISPR/Cas9 Screening Reveals Epistatic Networks of Interacting Tumor Suppressor Genes and Therapeutic Targets in Human Breast Cancer. Cancer Res. 2021;81(24):6090-105.

8. Nia A, Dhanasekaran R. Genomic Landscape of HCC. Curr Hepatol Rep. 2020;19(4):448-61.

9. Liu Y, Qi X, Zeng Z et al. CRISPR/Cas9-mediated p53 and Pten dual mutation accelerates hepatocarcinogenesis in adult hepatitis B virus transgenic mice. Sci Rep. 2017;7(1):2796.

10. Feldser DM, Kostova KK, Winslow MM et al. Stage-specific sensitivity to p53 restoration during lung cancer progression. Nature. 2010;468(7323):572-5.

11. Horie Y, Suzuki A, Kataoka E et al. Hepatocyte-specific Pten deficiency results in steatohepatitis and hepatocellular carcinomas. J Clin Invest. 2004;113(12):1774-83.

12. Ong CK, Subimerb C, Pairojkul C et al. Exome sequencing of liver fluke-associated cholangiocarcinoma. Nat Genet. 2012;44(6):690-3.

13. Reza HA, Okabe R, Takebe T. Organoid transplant approaches for the liver. Transpl Int. 2021;34(11):2031-45.

14. Prior N, Inacio P, Huch M. Liver organoids: from basic research to therapeutic applications. Gut. 2019;68(12):2228-37.

15. Huch M, Dorrell C, Boj SF et al. In vitro expansion of single Lgr5+ liver stem cells induced by Wnt-driven regeneration. Nature. 2013;494(7436):247-50.

16. Huch M, Gehart H, van Boxtel R et al. Long-term culture of genome-stable bipotent stem cells from adult human liver. Cell. 2015;160(1-2):299-312.

17. Vlachogiannis G, Hedayat S, Vatsiou A et al. Patient-derived organoids model treatment response of metastatic gastrointestinal cancers. Science. 2018;359(6378):920-6.

18. Park M, Kwon J, Kong J et al. A Patient-Derived Organoid-Based Radiosensitivity Model for the Prediction of Radiation Responses in Patients with Rectal Cancer. Cancers (Basel). 2021;13(15).

19. Percie du Sert N, Hurst V, Ahluwalia A et al. The ARRIVE guidelines 2.0: Updated guidelines for reporting animal research. Br J Pharmacol. 2020;177(16):3617-24.

20. National Research Council Committee for the Update of the Guide for the C, Use of Laboratory A. The National Academies Collection: Reports funded by National Institutes of Health. Guide for the Care and Use of Laboratory Animals. Washington (DC): National Academies Press (US)

Copyright © 2011, National Academy of Sciences.; 2011.

21. Xue W, Chen S, Yin H et al. CRISPR-mediated direct mutation of cancer genes in the mouse liver. Nature. 2014;514(7522):380-4.

22. An SB, Yang K, Kim CW et al. Longitudinal Imaging of Liver Cancer Using MicroCT and Nanoparticle Contrast Agents in CRISPR/Cas9-Induced Liver Cancer Mouse Model. Technol Cancer Res Treat. 2021;20:15330338211016466.

23. Navarro KL, Huss M, Smith JC, Sharp P, Marx JO, Pacharinsak C. Mouse Anesthesia: The Art and Science. ILAR Journal. 2021;62(1-2):238-73.

24. Moore DF, SpringerLink (Online service). Applied Survival Analysis Using R. Use R!,. p. XIV, 226 p. 66 illus., 26 illus. in color.

25. Therneau TM, Grambsch PM. Modeling survival data : extending the Cox model. New York: Springer; 2000.

26. Jung SB, Lee CY, Lee KH, Heo K, Choi SH. A cleavage-based surrogate reporter for the evaluation of CRISPR-Cas9 cleavage efficiency. Nucleic Acids Res. 2021;49(15):e85.

27. Park J, Lim K, Kim JS, Bae S. Cas-analyzer: an online tool for assessing genome editing results using NGS data. Bioinformatics. 2017;33(2):286-8.

28. Lim H, Jeong DH, Jang KW et al. Implementation of ultra-high dose-rate electron beam from 6-MeV C-band linear accelerator for preclinical study. Journal of Instrumentation. 2020;15(09):P09013.

29. Cancer Genome Atlas Research Network. Electronic address wbe, Cancer Genome Atlas Research N. Comprehensive and Integrative Genomic Characterization of Hepatocellular Carcinoma. Cell. 2017;169(7):1327-41 e23.

30. Xu H, Jiao D, Liu A, Wu K. Tumor organoids: applications in cancer modeling and potentials in precision medicine. J Hematol Oncol. 2022;15(1):58.

31. Ramakrishna G, Babu PE, Singh R, Trehanpati N. Application of CRISPR-Cas9 based gene editing to study the pathogenesis of colon and liver cancer using organoids. Hepatol Int. 2021;15(6):1309-17.

32. Zhang N, Bai H, David KK et al. The Merlin/NF2 tumor suppressor functions through the YAP oncoprotein to regulate tissue homeostasis in mammals. Dev Cell. 2010;19(1):27-38.

33. Zhang N, Zhao Z, Long J et al. Molecular alterations of the NF2 gene in hepatocellular carcinoma and intrahepatic cholangiocarcinoma. Oncol Rep. 2017;38(6):3650-8.

34. Chiasson-MacKenzie C, Morris ZS, Baca Q et al. NF2/Merlin mediates contact-dependent inhibition of EGFR mobility and internalization via cortical actomyosin. J Cell Biol. 2015;211(2):391-405.

35. Kato T, Murata D, Anders RA, Sesaki H, Iijima M. Nuclear PTEN and p53 suppress stress-induced liver cancer through distinct mechanisms. Biochem Biophys Res Commun. 2021;549:83-90.

36. Urtasun R, Latasa MU, Demartis MI et al. Connective tissue growth factor autocriny in human hepatocellular carcinoma: oncogenic role and regulation by epidermal growth factor receptor/yes-associated protein-mediated activation. Hepatology. 2011;54(6):2149-58.

37. Nuciforo S, Fofana I, Matter MS et al. Organoid Models of Human Liver Cancers Derived from Tumor Needle Biopsies. Cell Rep. 2018;24(5):1363-76.

38. Meier MA, Nuciforo S, Coto-Llerena M et al. Patient-derived tumor organoids for personalized medicine in a patient with rare hepatocellular carcinoma with neuroendocrine differentiation: a case report. Commun Med (Lond). 2022;2:80.

39. De Crignis E, Hossain T, Romal S et al. Application of human liver organoids as a patient-derived primary model for HBV infection and related hepatocellular carcinoma. Elife. 2021;10.

40. Schrag D, Weiser MR, Goodman KA et al. Neoadjuvant chemotherapy without routine use of radiation therapy for patients with locally advanced rectal cancer: a pilot trial. J Clin Oncol. 2014;32(6):513-8.

# Acknowledgement

This study was supported by the Dongnam Institute of Radiological and Medical Sciences (DIRAMS) grant funded by the Korea government (MSIT) (50495-2022, 50592-2022, 50493-2023, 50591-2023). This work was supported by the National Research Foundation of Korea (NRF) grant funded by the Korea government (MSIT) (No.2021R1A2C1095736, No. 2022R1A2C1092928).

# 국문초록

암 치료법의 개발로서 오가노이드는 최근 다양한 연구 분야에서 사용되고 있다. 특정 유전자 변이를 통한 암 오가노이드 모델의 생성은 환자 치료에 있어 새로운 지평선을 열어주고 있다. 본 연구에서는 다양한 유전적 돌연변이가 있는 간 종양의 방사선 반응성 탐색을 위해 *Tp53, Pten, Nf1, Nf2, Tsc2, Cdkn2a,* 또는 *Rb1* 유전자를 타겟으로 하는 Single-guide RNA를 이용한 크리스퍼 유전자 가위의 hydrodynamic injection을 통해 마우스 간 종양을 생성, 방사선 조사에 따른 반응성을 탐색하였다.

플라스미드 벡터는 성체 C57BL/6 마우스의 꼬리에 hydrodynamic injection을 통해 주입되었다. 각 그룹별 총 10마리의 마우스에 주입하였다. 이 그룹 중 간 종양이 확인된 마우스를 대상으로 오가노이드를 생성하였다. 오가노이드에 대한 방사선 반응성은 ATP 세포 생존 방법을 통해 평가하였다.

*Nf2* 유전자를 타겟으로 하는 마우스의 생존기간이 (4.8개월) 다른 마우스 군에 비해 짧은 것으로 나타났다. 헤마톡실린-에오신 염색, 면역조직화학염색, 타겟 염기서열분석에서 마우스 간 종양이 예측된 유전자 변이를 보이는 것이 확인되었다. 이러한 마우스 간 종양을 통해 각 군별 오가노이드를 구축하였다. 조직학적 분석에서 마우스 간 종양과 생성된

종양 오가노이드 사이에는 비슷한 형태학적 유사성을 보여주었다. 추가로 면역조직화학 염색에서도 마우스 간 종양과 오가노이드가 동일한 염색 패턴이 유지됨을 확인하였다. ATP 세포 생존 분석에서는 다른 변이 대비 *Nf2* 유전자 변이가 이뤄진 간 종양 오가노이드가 고선량 방사선에 저항성을 보이는 것이 확인되었다.

본 연구에서는 크리스퍼 유전자 가위를 이용, 마우스 간 종양 생성을 통해 특정 유전자의 변이가 가능함을 확인하였으며 마우스 간 종양 오가노이드의 방사선 조사량에 따른 반응을 탐색할 수 있었다. 특히 *Tp53, Pten* 그리고 *Nf2* 유전자의 동시 변화가 이뤄진 오가노이드의 경우 방사선 저항성이 증대됨을 확인하였다. 이러한 시스템은 향후 개별 간 종양의 유전자 변이에 따른 방사선 치료 반응성을 미리 예측할 수 있는 방법으로 고려될 수 있다.

**주요어: 크리스퍼 유전자 가위, 간, 오가노이드, 방사선저항성, 종양**

**학 번:** 2017-38794